RSOA Intensity Modulator Frequency Chirp-Enhanced Optical OFDM PON Performance

Tang, J.; Cao, B.; Deng, M.; Cao, B.Y.; Deng, M.L.; Zhang, Q.W.; Giddings, R.P.; Wang, M.

IEEE Photonics Journal

DOI:
10.1109/JPHOT.2015.2439261

Published: 05/06/2015

Publisher's PDF, also known as Version of record

IEEE Photonics Journal
An IEEE Photonics Society Publication

Open Access

RSOA Intensity Modulator Frequency Chirp-Enhanced Optical OFDM PON Performance

Volume 7, Number 3, June 2015

B. Y. Cao
M. L. Deng
Q. W. Zhang
R. P. Giddings
M. Wang
J. M. Tang

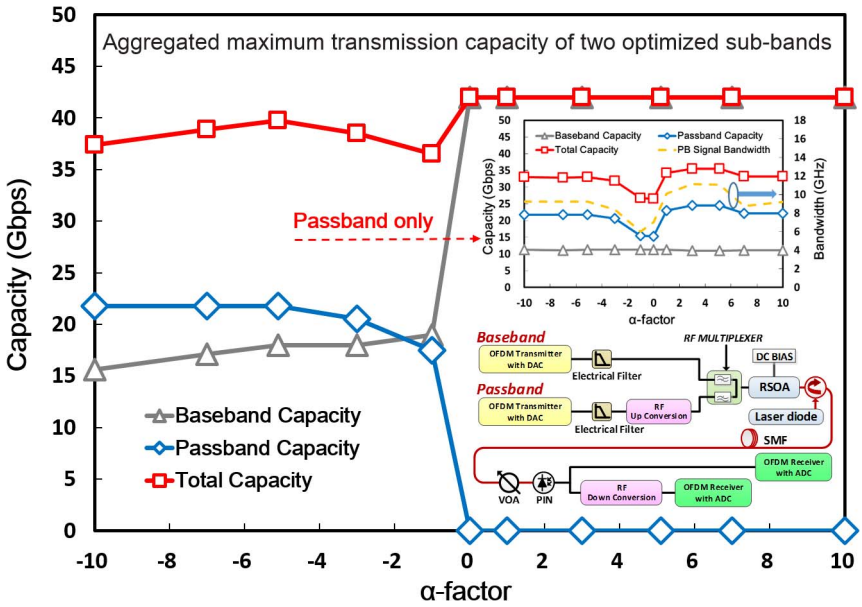

DOI: 10.1109/JPHOT.2015.2439261
1943-0655

IEEE photonics SOCIETY

IEEE

RSOA Intensity Modulator Frequency Chirp-Enhanced Optical OFDM PON Performance

B. Y. Cao,[1,2] M. L. Deng,[2,3] Q. W. Zhang,[1] R. P. Giddings,[2] M. Wang,[1] and J. M. Tang[2]

[1]Key Laboratory of Specialty Fiber Optics and Optical Access Networks, Shanghai University, Shanghai 200072, China
[2]School of Electronic Engineering, Bangor University, Bangor LL57 1UT, U.K.
[3]Key Laboratory of Optical Fiber Sensing and Communication Networks, University of Electronic Science and Technology of China, Chengdu 611731, China

DOI: 10.1109/JPHOT.2015.2439261

Manuscript received March 30, 2015; revised May 27, 2015; accepted May 27, 2015. Date of publication June 5, 2015; date of current version June 10, 2015. This work was supported in part by the Sino-U.K. Higher Education Research Partnership for Ph.D. Studies; by the Sêr Cymru National Research Network in Advanced Engineering and Materials; by the program of the Natural Science Foundation of China under Grant 61132004, Grant 61275073, and Grant 61420106011; and by the Shanghai Science and Technology Development Funds under Grant 13JC1402600 and Grant 14511100100. Corresponding author: J. M. Tang (e-mail: j.tang@bangor.ac.uk).

Abstract: A reflective semiconductor optical amplifier intensity modulator (RSOA-IM) frequency chirp considerably increases the system frequency response of an intensity-modulation and direct-detection (IMDD) PON system over the passband signal spectral region. Adaptive bit and power loading of optical OFDM (OOFDM) enables full use of the RSOA-IM frequency chirp-enhanced passband system frequency response characteristics. As a direct result, without requiring extra electrical and optical equalization schemes, an RSOA-IM with a 3-dB small-signal modulation bandwidth as low as 1 GHz can support 40 Gb/s OOFDM signal transmissions over 25 km SSMF IMDD PON systems free from optical amplification and chromatic dispersion compensation. This paper suggests that significantly relaxed requirements on both RSOA-IM's 3-dB small-signal modulation bandwidth and frequency chirp are feasible for achieving desired OOFDM transmission performances for next-generation PONs.

Index Terms: Reflective semiconductor optical amplifiers (RSOAs), frequency chirp, fiber optics systems, orthogonal frequency-division multiplexing (OFDM).

1. Introduction

Since reflective semiconductor optical amplifier-based intensity modulators (RSOA-IMs) have a large number of salient advantages including colorlessness, cost-effectiveness, compactness, low power dissipation, large-scale monolithic integration capability, as well as highly desirable functionalities of simultaneous signal modulation and amplification [1]–[4], RSOA-IMs are widely considered as cost-effective intensity modulator candidates for cost-sensitive application scenarios such as optical network units (ONUs) in next-generation passive optical networks (PONs) [5]–[7]. Commercially available, low-cost RSOAs have, however, very limited 3-dB small-signal modulation bandwidths, and the RSOA-IMs also suffer from the intensity modulation-induced strong frequency chirp effect [8]–[10], which may cause deep system frequency response nulls

to occur over the useful signal spectral regions in representative standard single-mode fiber (SSMF) PON systems based on intensity-modulation and direct-detection (IMDD) [10]. Inevitably, the aforementioned two unwanted features considerably degrade the transmission performance of the SSMF IMDD PON systems utilizing conventional signal modulation techniques.

To effectively combat the narrow small-signal modulation bandwidths of commercially available RSOAs, the utilization of highly spectral efficient and adaptive optical orthogonal frequency division multiplexing (OOFDM) is significantly advantageous [11]. In addition, to further address the performance degradations associated with both RSOA-IM's low small-signal modulation bandwidths and their large frequency chirps, use can also be made of the following two technical approaches: a) electrical equalization at either transmitters [12] or receivers [2], and b) optical equalization utilizing transmitter-side wavelength-offset optical filters [13] or receiver-side delay interferometers [14]. Both the electrical and optical equalization approaches are, however, strongly transmission system-dependent, thus imposing significant difficulties for practical realization of universal transceivers applicable in a wide diversity of PON application scenarios.

To enhance the RSOA-IM-based transceiver's flexibility and adaptability, as well as to simultaneously improve their transmission performances, a dual-band OOFDM transceiver configuration has been proposed [15], in which adaptively modulated baseband and passband OFDM signals are independently generated and electrically frequency-division-multiplexed (FDM) for intensity modulation of a single optical carrier in a RSOA-IM. Apart from the aforementioned considerably improved transmission performance, the dual-band OOFDM transceiver is also capable of not only reducing component inventory and digital signal processing (DSP) complexity, but also considerably relaxing the requirements on key transceiver component bandwidths. As a direct result, aggregated 17.125 Gb/s end-to-end real-time dual-band OOFDM transceivers have been experimentally demonstrated utilizing 1 GHz RSOA-IMs and digital-to-analog converters (DACs)/analog-to-digital converters (ADCs) operating at sampling speeds as low as 4 GS/s [15]. Both the strong adaptability and sufficiently large passband RF carrier frequency tunability of the experimentally demonstrated dual-band OOFDM transceiver enable full utilization of the highly dynamic spectral characteristics of the SSMF IMDD PON systems. This gives rise to the excellent transceiver performance robustness to variations in component operating conditions and system configurations.

The experimental results presented in [15] raise two very interesting open questions: a) whether or not the highly dynamic RSOA-IM frequency chirp can be used directly to enhance the transceiver performance, via DSP without introducing any extra analogue electrical/optical components in the entire OOFDM IMDD PON systems; b) if the answer to the first open question is positive, what is the maximum OOFDM transmission capacity achievable for such systems? The thrust of the present paper is to explore simple and effective answers to these two open questions, which are very valuable for practical PON system designs.

As a significant extension to our conference paper presented in [16] in terms of descriptions of experimental results-fitting procedures and resulting RSOA-IM microscopic parameters, and discussions of various physical mechanisms underpinning the RSOA-IM dynamic transmission performances, in this paper, based on rigorously verified theoretical models, extensive numerical explorations are undertaken of the transmission performances of RSOA-IM-based 17.125 Gb/s dual-band OOFDM transceivers over 25 km SSMF IMDD PON systems. For various RSOA-IM operating conditions and different PON system configurations, excellent agreements are obtained between simulated results and experimental measurements [15]. This enables the identification of a set of highly accurate RSOA-IM microscopic parameters. Making use of the identified RSOA-IM microscopic parameters, further investigations show that RSOA-IM frequency chirp-induced enhancements in system frequency response over the passband spectral region can considerably improve the aggregated dual-band OOFDM transmission capacity when adaptive bit and power loading is applied. In addition, it is also shown that adaptive bit and power loading enables RSOA-IMs to successfully intensity-modulate dual-band OOFDM signals having their bandwidths far beyond the RSOA's 3-dB small-signal modulation bandwidths specified by their manufacturers. Furthermore, numerical results also indicate that 1 GHz RSOA-IMs can support

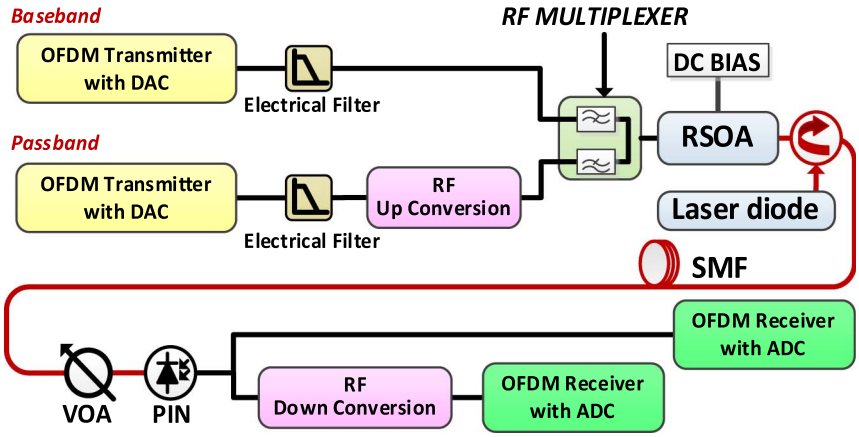

Fig. 1. Dual-band OOFDM IMDD PON system incorporating an RSOA-IM.

40 Gb/s adaptive OOFDM transmissions over 25 km SSMF IMDD PON systems without requiring extra analog electrical/optical equalization schemes, optical amplification, and chromatic dispersion compensation.

2. Transmission System and Experimental Result Fitting-Enabled RSOA-IM Microscopic Parameter Identification

2.1. Descriptions of Dual-Band OOFDM Transceiver and Transmission System

Fig. 1 illustrates the considered RSOA-IM-based dual-band OOFDM IMDD PON system, whose configuration is identical to that reported in [15], except that, for each individual signal band in the transmitter, an electrical filter is introduced to take into account the measured system frequency response roll-off effect associated with the analog electrical back-to-back transceiver configuration [15]. For digitally generating each signal band, detailed OFDM DSP functions can be found in [15], which include, for example, pseudo-random data generation, pilot-tone insertion, adaptive bit and power loading for 15 data-carrying subcarriers with signal modulation formats selected from 16-quadrature amplitude modulation (QAM), 32-QAM, and 64-QAM, a 32-point inverse fast Fourier transform (IFFT) with input complex data being arranged to satisfy the Hermitian symmetry, signal clipping level optimization, 8-bit sample quantization and cyclic prefix insertion. The adopted parameters of the key transceiver components and corresponding transmission system are presented in Table 1.

At the transmitter, a real-valued baseband OFDM signal emerging from a DAC passes through an electrical filter, whereas a double-sideband passband OFDM signal is produced by amplitude-modulating a RF carrier with another independently generated, real-valued OFDM baseband signal. After appropriately adjusting the signal power levels of both signal bands, these two signal bands are combined in a low-loss RF multiplexer. After that, the analog dual-band electrical OFDM signal is combined with an optimum DC bias current to directly modulate a 1550 nm CW optical wave in a 1 GHz RSOA-IM. The output optical power from the RSOA-IM is finely adjusted and subsequently injected into a 25 km SSMF IMDD PON system without optical amplification and chromatic dispersion compensation.

At the receiver, the optical signal passes through a variable optical attenuator (VOA) to adjust the received optical power. A 12.4 GHz PIN is employed to convert the received dual-band OOFDM signal into the electrical domain. To recover the baseband (passband) OFDM signal, the RF down-conversion operation illustrated in Fig. 1 is omitted (included), whose main functionalities consist of the estimations of the RF carrier frequency and phase offset, as well as corresponding RF carrier frequency/phase offset compensations. Finally, the received baseband signal and/or the down-converted passband signal is transferred to the receiver block for data

TABLE 1

Transceiver and transmission system parameters

OFDM DSP Parameters	*Value*	*Unit*
IFFT/FFT points per band	32	
Data-carrying subcarriers per band	15	
Subcarrier frequency spacing	N*125	MHz
Adaptive modulation formats on all subcarriers of each band	16QAM, 32QAM, 64QAM	
DAC & ADC sample rate	4	GS/s
DAC & ADC bit resolution	8	Bits
OFDM symbol rate	100	MHz
Samples per symbol (IFFT/FFT)	32	Samples
Cyclic prefix	8	Samples
Total samples per symbol	40	Samples
RSOA operating conditions		
3-dB input optical saturation power	-10	dBm
Passband RF carrier frequency	6.5	GHz
Bias current	81.87	mA
Driving voltage	3.4	Vpp
CW optical power injected into the RSOA	4.56	dBm
Launched optical power	10.4	dBm
PIN Parameters		
Detector bandwidth	12.4	GHz
Detector sensitivity[1]	-17	dBm
Fibre Parameters		
Length	25	km
Type	SSMF	
Dispersion	17	ps/nm/km
Dispersion slope	0.07	ps/nm/km
Loss	0.22	dB/km
Kerr coefficient	2.35e-20	m^2/W

[1] Corresponding to 10 Gb/s non-return-to-zero data at a BER of 1.0×10^{-9}

recovery utilizing conventional OFDM receiver DSP procedures including symbol synchronization, pilot-subcarrier detection, and channel estimation/equalization. All other remaining receiver DSP functions are just inverse to their transmitter DSP counterparts [15].

2.2. Theoretical Models and RSOA-IM Microscopic Parameter Identification Procedures

For accurately simulating the transmission performance of the PON system of interest of the present paper, a number of comprehensive theoretical models developed and evaluated in [17] are adopted, which include a) an OFDM transceiver model with adaptive subcarrier bit and power loading; b) a RSOA-IM model with injected optical power- and wavelength-dependent dynamics of optical gain and ASE; c) a standard SSMF transmission model incorporating the effects of loss, chromatic dispersion and various fiber nonlinearities; and d) a square-law photon detection model with both shot and thermal noises being present. The validity of all these theoretical models has been rigorously verified at both component and system levels [17].

To accurately predict the OOFDM transmission performance for various component operating conditions and PON system configurations, in our numerical simulations, all the parameters of the components and PON system, which have already been made known in our previous experiments [15], are adopted and remain constant for all cases considered in the paper. A full list of those parameters is presented in Table 1, which consists of the following four sections: a) core transceiver DSP function-related parameters including signal modulation formats, number of

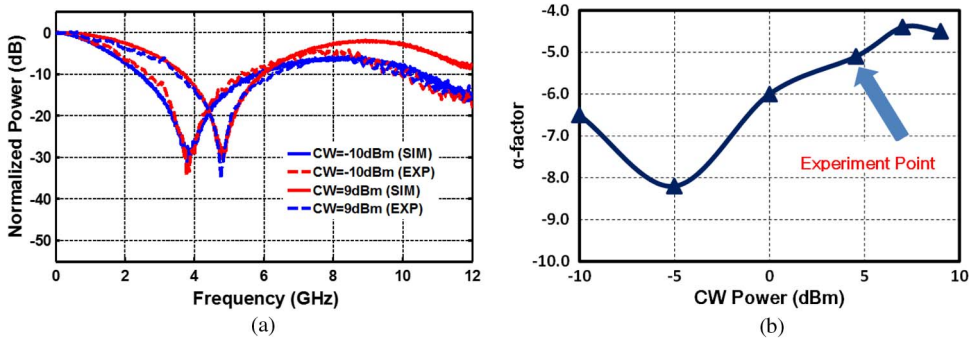

Fig. 2. (a) Calculated and experimentally measured fiber transfer functions for the RSOA-IM subject to two injected CW optical powers of 9 dBm and −10 dBm. (b) Injected CW optical power-dependent α-factor of the RSOA-IM.

subcarriers of each band, DAC/ADC sampling rates and quantization bits; b) RSOA-IM operating condition-related parameters including input optical saturation power, bias current, peak-to-peak driving current and CW optical power injected into the RSOA-IM; c) photon detection-related parameters including receiver bandwidth and sensitivity; and d) typical SSMF fiber parameters that are widely adopted. It should be noted that both the noise figure and the carrier lifetime of the employed RSOA-IM are strongly operating condition-dependent: With increasing the optical input power, the noise figure increases and the carrier lifetime decreases [17].

Given the central role of the RSOA-IM in determining the PON system performance, special attention is also given to the accuracy of its unknown microscopic parameters. The initial values of the RSOA-IM's microscopic parameters are first chosen from [17], during experimental result fitting, those parameter values are then finely adjusted within their reasonable dynamic ranges to ensure the best fitting between simulated results and experimental measurements is obtained in terms of both bit error rate (BER) and/or signal transmission capacity for various RSOA-IM operating conditions and transmission system configurations.

It should also be noted, in particular, that the RSOA-IM linewidth enhancement factor, here termed α-factor, is highly intensity modulator operating condition-dependent, and plays a dominant role in governing the dynamic RSOA-IM frequency chirp characteristics. The α-factor satisfies [10]

$$H(\omega) = \left|\cos(\theta) - \sin(\theta)\alpha\left(1 - j\frac{\omega_c}{\omega}\right)\right| \quad \text{with } \theta = \frac{LD\lambda^2\omega^2}{4\pi c} \text{ and } \omega_c = \kappa P_0 \tag{1}$$

where $H(\omega)$ is the fiber transfer function contributed by a fiber section ranging from the optical transmitter output to the optical receiver input; θ is a function of fiber length L, fiber dispersion parameter D, central wavelength λ, and signal frequency ω; κ is the adiabatic frequency chirp coefficient, and P_0 is the average optical power injected into the fiber. Assuming a fixed fiber section with its relevant parameters made known, for optical signals modulated by the RSOA-IM subject to various CW optical powers, from (1), the injected CW optical power-dependent α-factor can be easily worked out utilizing precisely measured frequencies corresponding to the nulls of the fiber transfer function. Therefore, the measured optical power dependent α-factor values are employed in numerical simulations.

2.3. Experimental Result Fitting and Identified RSOA-IM Microscopic Parameters

Utilizing the theoretical models and the parameter identification procedures described in Section 2.2, in this section, detailed simulations are undertaken to numerically fit all the results experimentally measured in [15]. Fig. 2(a) shows the calculated and experimentally measured fiber transfer functions normalized to the power level corresponding to the zero reference frequency. In Fig. 2(a), two representative CW optical powers injected into the RSOA-IM, i.e.,

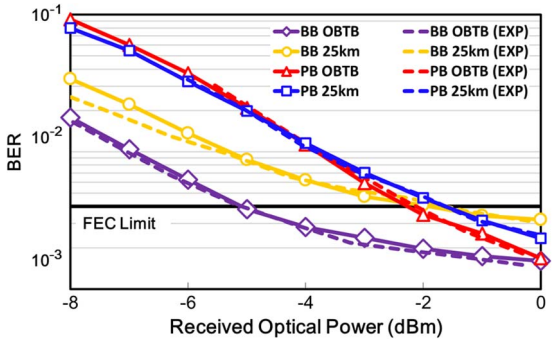

Fig. 3. Numerically fitted and experimentally measured BER performances of the 11.25 Gb/s baseband and the 6 Gb/s passband for optical back-to-back and 25 km SSMF IMDD PON systems utilizing the RSOA-IM.

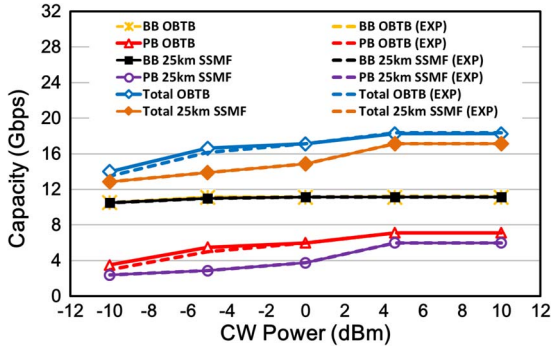

Fig. 4. Numerically fitted and experimentally measured transmission capacity of each individual signal band versus CW optical power injected into the RSOA-IM when full parameter optimization is applied. Both optical back-to-back and 25 km SSMF PON systems are considered.

-10 dBm and 9 dBm, are shown, as they represent the minimum and maximum values of the CW optical power dynamic range considered in the paper. Within such an optical power dynamic range, the RSOA-IM is strongly saturated, thus resulting in very low optical gains in the vicinity of 0 dB. As a result, a strong optical power-dependent α-factor behavior calculated using (1) is observed in Fig. 2(b). It can also be seen in Fig. 2(b) that the CW optical power of 4.56 dBm adopted in [15] corresponds to a α-factor value of -5.1.

Making use of the subcarrier bit and power loading profiles identical to those reported in [15], Fig. 3 shows the numerically fitted and experimentally measured BER performances of the 11.25 Gb/s baseband and 6 Gb/s passband for both the optical back-to-back and entire 25 km SSMF IMDD PON systems. To satisfy the power budget requirements of practical PON transmission systems, the PIN employed here can be replaced by an APD with a power sensitivity of -28 dBm. It has been shown experimentally [15] that such a simple detector replacement results in an approximately 7 dB improvement in receiver sensitivity for both sub-bands. In addition, a further 7 dB receiver sensitivity improvement may also be achievable when use is made of wavelength-offset Gaussian filtering at the output of the RSOA-IM [18].

For system configurations very similar to Figs. 3 and 4 presents the numerically fitted and experimentally measured maximum signal transmission capacity of each signal band versus CW optical power injected into the RSOA-IM. Similar to the experimental procedures adopted in [15], in obtaining Fig. 4, for a specific optical power injection, extensive optimizations of all other controllable parameters are undertaken until the maximum signal transmission capacity for each individual band is achieved at a forward error correction (FEC) limit of 4.0×10^{-3}. These controllable parameters include subcarrier bit and power loading profiles for each band, electrical signal

TABLE 2

Fitted RSOA-IM microscopic parameters

Parameter	*Value*	*Units*
Cavity Length	300	
Width of active region	1.5	um
Depth of active region	0.27	um
Carrier lifetime at small-signal gain	0.33	ns
Confinement factor	0.45	
Differential Gain	3.3e-20	m^2
Carrier density at transparency	1.2e24	m^{-3}
Noise figure at small-signal gain	6.7	dB
RSOA rear-facet reflectivity	0.95	

power of each band, RSOA-IM bias/driving current, and passband RF carrier frequency. Of course, the CW optical power dependent α-factor behavior is also considered in simulating Fig. 4.

It can be seen in Figs. 2–4 that excellent agreements between the numerically simulated results and experimental measurements are obtained for various RSOA-IM operating conditions and transmission system configurations. This strongly confirms not only the validity of the adopted theoretical models but also the accuracy of the RSOA-IM microscopic parameter sets. The identified RSOA-IM microscopic parameter values are listed in Table 2. It should be noted that, together with the α-factor dynamics shown in Fig. 2(b), the parameters in Table 2 are employed as constant in simulating all results presented in Sections 3 and 4.

3. RSOA-IM Frequency Chirp-Enhanced Transmission Performance

Having identified the RSOA-IM microscopic parameters in Section 2, the main objectives of Section 3 are twofold: a) to examine the feasibility of utilizing the RSOA-IM frequency chirp to improve the aggregated OOFDM transmission capacity and b) to investigate the physical mechanisms responsible for the RSOA-IM frequency chirp-enhanced OOFDM transmission performance.

To address the abovementioned first objective, Fig. 5 is presented for various α-factors in a 25 km SSMF IMDD system. The simulated passband signal transmission capacities as a function of passband RF carrier frequency are shown in Fig. 5(a) and (b), in obtaining both of which adaptive bit and power loading is applied to each data-conveying subcarrier, and the CW optical power injected to the RSOA-IM varies according to the α-factor values adopted. In addition, as the baseband signal transmission capacity of 11.125 Gb/s is always obtainable for all the cases considered here, such a transmission capacity is thus excluded in Fig. 5(a) and (b). Corresponding to these transmission capacity figures, Fig. 5(c) and (d) shows normalized fiber transfer functions associated with different α-factors adopted.

In Fig. 5(a) and (b), it is very interesting to note that a large absolute value of α-factor always gives rise to a high passband signal transmission capacity. In addition, for each α-factor and over the considered passband spectral region, the passband signal capacity developing trend follows the variation of the fiber transfer function of the same α-factor. For example, in Fig. 5(b), for a α-factor value of -1 and a spectral range from 8 GHz to 10 GHz, a sudden drop of the passband signal capacity is observed as the consequence of the occurrence of a deep fiber transfer function null within the passband spectral region, as seen in Fig. 5(d). The abovementioned behaviors indicate that the passband can effectively utilize the RSOA-IM frequency chirp-induced increases in system frequency response over a wide passband spectral region.

To further explore the physical mechanisms underpinning the RSOA-IM frequency chirp-enhanced transmission performance, based on the simulation parameters identical to those used in Fig. 5 except that α is fixed at -5.1, Fig. 6 is presented to compare passband signal transmission capacities between different loading schemes namely, uniform bit and power loading, power loading only, bit loading only, and bit and power loading. In implementing these

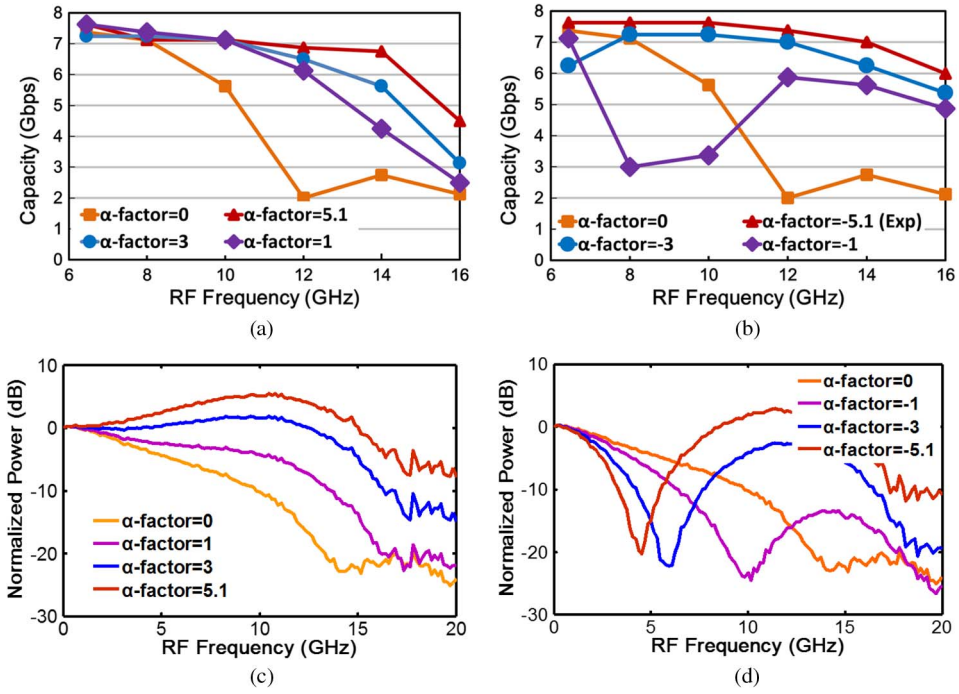

Fig. 5. (a) and (b) Passband signal transmission capacities for different α-factors. (c) and (d) Normalized fiber transfer functions for different α-factors.

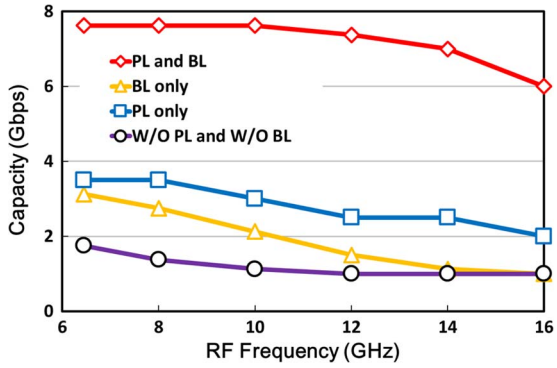

Fig. 6. Passband transmission capacity for different loading schemes. 25 km SSMF IMDD systems are considered, and α is fixed at -5.1. PL: power loading, BL: bit loading.

different loading schemes for each passband RF carrier frequency, a highest possible signal modulation format is always attempted and the total passband electrical power remains constant. It is very easy to see in Fig. 6 that bit and power loading is the dominant mechanism allowing the effective use of the RSOA-IM frequency chirp for the passband.

4. Maximum Achievable Signal Transmission Capacity

This section is to explore the maximum achievable signal transmission capacity of the 1 GHz RSOA-IM-based 25 km SSMF IMDD PON system when adaptive bit and power loading is adopted. To effectively address such a challenging task, extensive parameter optimizations of all experimentally controllable transceiver component parameters are undertaken until the maximum signal transmission capacity is achieved under a condition that the BER of the corresponding signal band is below the adopted FEC limit. Apart from adaptive subcarrier bit and power

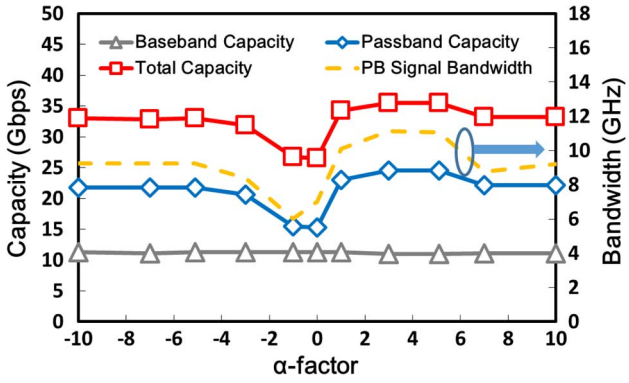

Fig. 7. Maximum achievable transmission capacity when transceiver component parameters associated with the passband are optimized only. 25 km SSMF IMDD PON systems are considered, and the baseband signal parameters are identical to those listed in Table 1.

loading, the optimized component parameters include ADC/DAC sampling rate, RSOA-IM-injected CW optical power (the α-factor varies accordingly), electrical power of each signal band and relative electrical powers between two signal bands, RSOA-IM bias and driving currents, as well as passband RF carrier frequency. All remaining parameters that are not mentioned explicitly above are kept constant and their parameter values are taken from Table 1.

When the aforementioned parameter optimizations are applied only to the passband signal with the baseband signal parameters kept identical to those shown in Table 1, Fig. 7 represents the resulting maximum achievable transmission capacity over the 25 km SSMF IMDD PON system. In simulating Fig. 7, it is found that both the ADC/DAC sampling rate and adaptive bit/power loading are very critical in determining the maximum achievable signal transmission capacity, and that the ADC/DAC sampling rates varying from 8 GS/s to 16 GS/s are sufficient to enable the passband signals to fully utilize the RSOA-IM frequency chirp-enhanced system frequency responses.

It can be seen in Fig. 7 that a maximum passband signal transmission capacity of 24.5 Gb/s is achievable, which gives rise to an aggregated transmission capacity of 35 Gb/s (the baseband signal transmission capacity always remains at 11.125 Gb/s). The aggregated maximum signal transmission capacity varies with the passband signal bandwidths determined by the ADC/DAC sampling rates. It can be understood from Fig. 5(d) that, for α-factors altering in a range from -3 to 1, deep system frequency response nulls occur in the passband spectral region, thus leading to a reduced passband signal capacity, as seen in Fig. 7.

On the other hand, when the parameter optimization operations are applied to both the baseband and the passband simultaneously, the simulated maximum achievable transmission capacity is given in Fig. 8, where the maximum ADC/DAC sampling rate still remains at 16 GS/s. In comparison with Fig. 7, the α-factor dependent aggregated signal capacity variation in Fig. 8 is significantly flattened, and more importantly, aggregated 40 Gb/s OOFDM transmission over 25 km SSMF IMDD PON systems are feasible. In Fig. 8, there also exist sharp changes in passband and baseband transmission capacities in the vicinity of zero α-factor, this is due to the fact that positive α-factors do not cause the system frequency response nulls to appear in the useful signal spectral region, as seen in Fig. 5(c), thus compared to the dual-band cases, a single band can achieve higher signal transmission capacities because the single band is free from the multi-band-induced crosstalk effect.

5. Conclusion

Utilizing rigorously verified theoretical models, extensive numerical simulations have been undertaken to fit experimentally measured, 1 GHz RSOA-IM-modulated, 17.125 Gb/s dual-band OOFDM transmissions over 25 km SSMF IMDD PON systems. For various RSOA-IM operating conditions and different PON system configurations, excellent agreements between the

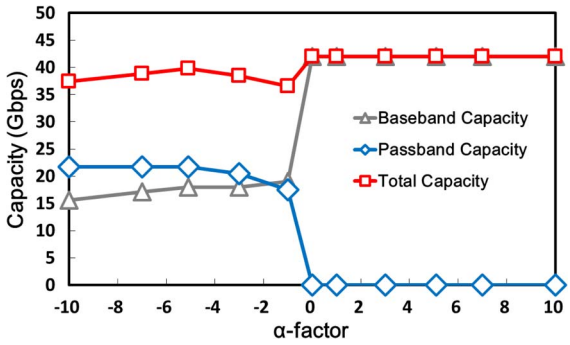

Fig. 8. Maximum achievable transmission capacity when transceiver component parameters associated with the baseband and passband are optimized. 25 km SSMF IMDD PON systems are considered.

simulated results and the experimental measurements have been observed, thus enabling the identification of a set of highly accurate RSOA-IM microscopic parameters. Making use of the identified parameters, further investigations have shown that RSOA-IM frequency chirp-induced enhancements in system frequency response can considerably improve the aggregated dual-band OOFDM transmission capacity when adaptive bit and power loading is applied. In addition, it has also been shown that adaptive bit and power loading enables RSOA-IMs to successfully intensity-modulate dual-band signals having their bandwidths far beyond the RSOA's 3-dB small-signal modulation bandwidths. Furthermore, our results have also indicated that 1 GHz RSOA-IMs can support 40 Gb/s adaptive OOFDM transmissions over 25 km SSMF IMDD PON systems without requiring extra analogue electrical/optical equalization schemes. The present work suggests that significantly relaxed requirements on both RSOA-IM modulation bandwidth and frequency chirp are feasible for achieving desired OOFDM transmission performances for next-generation PONs.

References

[1] C. H. Yeh, C. W. Chow, H. Y. Chen, and Y. F. Wu, "10-Gbps OFDM upstream rate by using RSOA-ONU with seeding-light for 75 km long-reach PON access," presented at the Nat. Fiber Opt. Eng. Conf., Los Angeles, CA, USA, 2012, Paper JTh2A.65.

[2] K. Cho, B. Choi, Y. Takushima, and Y. Chung, "25.78-Gb/s operation of RSOA for next-generation optical access networks," *IEEE Photon. Technol. Lett.*, vol. 23, no. 8, pp. 495–497, Apr. 2011.

[3] I. Cano, M. Omela, J. Prat, and P. Poggiolini, "Colorless 10 Gb/s extended reach WDM PON with low BW RSOA using MLSE," presented at the Nat. Fiber Opt. Eng. Conf., San Diego, CA, USA, 2010, Paper OWG2.

[4] J. Joo, M. Hong, D. Pham, and S. Han, "20-Gb/s adaptively modulated optical OFDM transmission over 20-km single fiber loopback WDM PON based on separated I/Q baseband delivery using 1 GHz RSOAs," presented at the Nat. Fiber Opt. Eng. Conf., Los Angeles, CA, USA, 2012, Paper JTh2A.31.

[5] M. Hong *et al.*, "10-Gb/s transmission over 20-km single fiber link using 1-GHz RSOA by discrete multitone with multiple access," *Opt. Exp.*, vol. 19, no. 26, pp. B486–B495, Dec. 2011.

[6] N. Cvijetic *et al.*, "Terabit optical access networks based on WDM-OFDMA-PON," *J. Lightw. Technol.*, vol. 30, no. 4, pp. 493–503, Feb. 2012.

[7] P. Vetter, "Next generation optical access technologies," presented at the Eur. Conf. Exhib. Opt. Commun., Amsterdam, The Netherlands, 2012, Paper Tu.3.G.

[8] I. Papagiannakis *et al.*, "Upstream transmission in WDM PONs at 10 Gb/s using low bandwidth RSOAs assisted with optical filtering and electronic equalization," presented at the Eur. Conf. Exhib. Optical Commun., Brussels, Belgium, 2008, Paper We.3.F.3.

[9] T. Duong *et al.*, "Experimental demonstration of 10 Gbit/s for upstream transmission by remote modulation of 1 GHz RSOA using adaptively modulated optical OFDM for WDM-PON single fiber architecture," presented at the Eur. Conf. Exhib. Opt. Commun., Brussels, Belgium, 2008, Paper Th.3.F.1.

[10] L. A. Neto *et al.*, "Simple estimation of fiber dispersion and laser chirp parameters using the downhill simplex fitting algorithm," *J. Lightw. Technol.*, vol. 31, no. 2, pp. 334–342, Jan. 2013.

[11] R. Giddings, "Real-time digital signal processing for optical OFDM-based future optical access networks," *J. Lightw. Technol.*, vol. 32, no. 4, pp. 553–570, Feb. 2014.

[12] B. Schrenk *et al.*, "Direct 10-Gb/s modulation of a single-section RSOA in PONs with high optical budget," *IEEE Photon. Technol. Lett.*, vol. 22, no. 6, pp. 392–394, Mar. 2010.

[13] G. Cossu, F. Bottoni, R. Corsini, M. Presi, and E. Ciaramella, "40 Gb/s single R-SOA transmission by optical equalization and adaptive OFDM," *IEEE Photon. Technol. Lett.*, vol. 25, no. 21, pp. 2119–2122, Nov. 2013.
[14] H. Kim, "10-Gb/s operation of RSOA using a delay interferometer," *IEEE Photon. Technol. Lett.*, vol. 22, no. 18, pp. 1379–1381, Sep. 2010.
[15] Q. W. Zhang *et al.*, "Record-high and robust 17.125 Gb/s gross-rate over 25 km SSMF transmissions of real-time dual-band optical OFDM signals directly modulated by 1 GHz RSOAs," *Opt. Exp.*, vol. 22, no. 6, pp. 6339–6348, Mar. 2014.
[16] B. Y. Cao *et al.*, "RSOA intensity modulator frequency chirp-enabled 40 Gb/s over 25 km IMDD PON systems," presented at the Opt. Fiber Commun. Conf., Los Angeles, CA, USA, 2015, Paper W1J.3.
[17] J. L. Wei *et al.*, "Adaptively modulated optical OFDM modems utilizing RSOAs as intensity modulators in IMDD SMF transmission systems," *Opt. Exp.*, vol. 18, no. 8, pp. 8556–8573, Apr. 2010.
[18] J. L. Wei, C. Sánchez, R. P. Giddings, E. Hugues-Salas, and J. M. Tang, "Significant improvements in optical power budgets of real-time optical OFDM PON systems," *Opt. Exp.*, vol. 18, no. 20, pp. 20 732–20 745, Sep. 2010.